

# UC Davis

## UC Davis Previously Published Works

### Title

Preclinical Dose-Escalation Study of Intravitreal AAV-RS1 Gene Therapy in a Mouse Model of X-linked Retinoschisis: Dose-Dependent Expression and Improved Retinal Structure and Function

### Permalink

<https://escholarship.org/uc/item/69p0m878>

### Journal

Human Gene Therapy, 27(5)

### ISSN

2324-8637

### Authors

Bush, Ronald A  
Zeng, Yong  
Colosi, Peter  
et al.

### Publication Date

2016-05-01

### DOI

10.1089/hum.2015.142

Peer reviewed

# Preclinical Dose-Escalation Study of Intravitreal AAV-RS1 Gene Therapy in a Mouse Model of X-linked Retinoschisis: Dose-Dependent Expression and Improved Retinal Structure and Function

Ronald A. Bush,<sup>1,†,\*</sup> Yong Zeng,<sup>1,†</sup> Peter Colosi,<sup>2</sup> Sten Kjellstrom,<sup>1,3</sup> Suja Hiriyanna,<sup>2</sup> Camasamudram Vijayasarathy,<sup>1</sup> Maria Santos,<sup>2</sup> Jinbo Li,<sup>1</sup> Zhijian Wu,<sup>2</sup> and Paul A. Sieving<sup>1,2</sup>

<sup>1</sup>National Institute on Deafness and Other Communication Disorders and <sup>2</sup>National Eye Institute, National Institutes of Health, Bethesda, Maryland; <sup>3</sup>Department of Ophthalmology, Lund University, Lund, Sweden.

<sup>†</sup>These two authors contributed equally to this work.

Gene therapy for inherited retinal diseases has been shown to ameliorate functional and structural defects in both animal models and in human clinical trials. X-linked retinoschisis (XLRS) is an early-age onset macular dystrophy resulting from loss of an extracellular matrix protein (RS1). In preparation for a human clinical gene therapy trial, we conducted a dose-range efficacy study of the clinical vector, a self-complementary AAV delivering a human retinoschisin (*RS1*) gene under control of the *RS1* promoter and an interphotoreceptor binding protein enhancer (AAV8-scRS/IRBPhRS), in the retinoschisin knockout (*Rs1*-KO) mouse. The therapeutic vector at  $1 \times 10^6$  to  $2.5 \times 10^9$  (1E6–2.5E9) vector genomes (vg)/eye or vehicle was administered to one eye of 229 male *Rs1*-KO mice by intravitreal injection at  $22 \pm 3$  days postnatal age (PN). Analysis of retinal function (dark-adapted electroretinogram, ERG), structure (cavities and outer nuclear layer thickness) by *in vivo* retinal imaging using optical coherence tomography, and retinal immunohistochemistry (IHC) for RS1 was done 3–4 months and/or 6–9 months postinjection (PI). RS1 IHC staining was dose dependent across doses  $\geq 1E7$  vg/eye, and the threshold for significant improvement in all measures of retinal structure and function was 1E8 vg/eye. Higher doses, however, did not produce additional improvement. At all doses showing efficacy, RS1 staining in *Rs1*-KO mouse was less than that in wild-type mice. Improvement in the ERG and RS1 staining was unchanged or greater at 6–9 months than at 3–4 months PI. This study demonstrates that vitreal administration of AAV8 scRS/IRBPhRS produces significant improvement in retinal structure and function in the mouse model of XLRS over a vector dose range that can be extended to a human trial. It indicates that a fully normal level of RS1 expression is not necessary for a therapeutic effect.

## INTRODUCTION

THE SUCCESS OF PRECLINICAL STUDIES and phase I and phase II clinical trials for Leber congenital amaurosis (LCA)<sup>1–6</sup> provided proof-of-principle that gene transfer is a viable approach for treatment of inherited retinal degeneration. One of these has now moved into phase III.<sup>7</sup> Gene therapy for a number of other retinal diseases has shown sufficient promise in preclinical studies that several phase I clinical trials have begun (choroideremia: NCT01461213; Stargardt disease: NCT01367444; Usher syndrome: NCT02065011, NCT01505062).

All of these trials deliver the therapeutic vector to the subretinal space, which requires a complex surgical intervention. Recently, a trial of gene therapy for Leber hereditary optic neuropathy (LHON) was completed using an intravitreal injection (NCT01267422). Here we document a dosing efficacy study in the mouse model of X-linked retinoschisis (XLRS) that resulted in FDA approval of a phase I/II dose-escalation clinical trial (ClinicalTrials.gov No. NCT02317887) in which the clinical lead vector was administered by a single injection into the vitreous.

\*Correspondence: Dr. Ronald A. Bush, 50 South Drive, Bethesda, MD 20892-8021. E-mail: bushr@nidcd.nih.gov

XLRS is an inherited retinal disease caused by mutations in an extracellular adhesion protein, retinoschisin (RS1), and is a relatively common form of macular degeneration in young males.<sup>8</sup> The structural phenotype includes splitting of retinal layers, which is most often seen in the fovea and macula but also is quite common in the peripheral retina.<sup>9</sup> It is accompanied by mild to severe vision loss, including reduced visual acuity, beginning at an early age. Being an X-linked recessive disease, it is passed from mothers to affected males, and female carriers nearly never display the disease phenotype. Optical coherence tomography (OCT) imaging and the electroretinogram (ERG) are the primary means for diagnosis and tracking disease progression. Retinal splitting produces “schisis cavities” seen in OCT images that occur primarily in layers proximal to photoreceptors. The ERG shows a characteristic “negative” waveform, in which the b-wave arising from bipolar cells postsynaptic to photoreceptors is greatly reduced in amplitude. The a-wave is much less affected or not reduced at all, resulting in a reduced b-wave-to-a-wave amplitude ratio. This ratio may decline further with age or remain relatively stationary depending on genotype.<sup>10</sup>

XLRS results from deficiency or defects in RS1. RS1 is a 224-amino-acid secreted protein that is expressed normally in the retina by photoreceptors and bipolar, amacrine, and ganglion cells.<sup>11–14</sup> It contains a single discoidin domain consistent with a key role in cell adhesion and interaction with collagens to regulate extracellular matrix modeling.<sup>11,15,16</sup> Thus, RS1 is thought to be critical for normal development and maintenance of retinal structure. In addition, evidence indicates that RS1 may be crucial for maintaining structural connection of postsynaptic elements in the outer plexiform layer (OPL) between photoreceptors and bipolar cells that is necessary for the transmission of visual signal.<sup>12,13,17,18</sup>

There are no known naturally occurring animal models of XLRS; hence, the retinoschisin knockout (*Rs1*-KO) mouse was developed by targeted gene disruption.<sup>19,20</sup> The mouse used in this study displays the features of the human disease, including retinal schisis cavities and reduced ERG b-wave/a-wave ratio, which can be ameliorated by gene replacement using intravitreal AAV delivery.<sup>20</sup> This model also shows a progression in the phenotype<sup>21</sup> similar to that seen in a recent cross-sectional analysis of 68 XLRS patients with “noticeably severe” mutations.<sup>10</sup> Thus, it serves as a good model of the disease for exploring the efficacy of a gene therapy vector.

An FDA application to conduct a clinical trial of an investigative new drug (IND) requires proof-of-concept studies that demonstrate benefit of the drug entity. The purpose is to explore the feasibility and rationale for the treatment in the targeted population and should include a demonstration of the pharmacologically effective dose range in an animal disease model using the same route of administration to be used in the clinical trial.<sup>22</sup> These studies are critical in setting the starting dose and the dosing range for the clinical trial.

The current study employs a self-complementary adeno-associated virus vector delivering the human *RS1* gene with a modified *RS1* promoter and IRBP enhancer to increase the speed, efficiency, and specificity of expression and thereby reduce the dose required and decrease potential toxicity. Using the *Rs1*-KO model, the efficacy of intravitreal injection of doses from  $1 \times 10^6$  to  $2.5 \times 10^9$  (1E6 to 2.5E9) vector genomes (vg)/eye was investigated. Doses from 1E8 to 2.5E9 vg/eye produced statistically significant improvement in retinal function and structure. Functional improvement was shown by increased ERG a-wave and b-wave amplitudes and b-wave/a-wave ratio at 3–4 months and 6–9 months post-injection (PI) relative to fellow untreated eyes. Structural improvement was shown by reduction of retinal cavities 3–4 months PI. The threshold for efficacy was 1E8 vg/eye, and immunohistochemistry (IHC) showed robust staining for RS1 at this dose but at a level lower than that in wild-type (WT) mice, suggesting that full expression is not necessary for efficacy. Interestingly, doses above the threshold for efficacy did not result in significantly better function or structure than seen at threshold, though RS1 staining continued to increase.

## METHODS

### Test article

The test article in this study, AAV8-scRS/IRBPhRS (AAV-RS1), and its manufacture were described previously.<sup>23</sup> Briefly, AAV-RS1 is an adeno-associated virus type 8 vector that delivers a self-complementary vector genome composed of a modified human retinoschisin promoter that drives expression of a human retinoschisin cDNA. This vector also employs an interphotoreceptor retinoid-binding protein (IRBP) enhancer to augment promoter activity, a truncated retinoschisin first intron located in its authentic position between exon 1 and 2 sequences and a human beta-globin 3' untranslated region and polyadenylation site. We are currently using the Good Manufacturing Practice (GMP) version of this therapeutic vector in

the human clinical trial (Clinical Trials. Gov. NCT 02317887).

### ***Rs1*-KO mouse**

The retinoschisin knockout (*Rs1*-KO) mouse model was generated as described previously.<sup>20</sup> These mice have been maintained at NIH since 2003 in a shared animal facility administered by the National Institute of Allergy and Infectious Diseases (NIAID) and backcrossed onto the C57BL/6J line (Jackson Laboratory). The phenotype and natural history of this animal have been previously described.<sup>18,20,21</sup> The present study included 229 male *Rs1*-KO mice from 60 litters that were the offspring of 26 different homozygous and 6 heterozygous female *Rs1*-KO mice crossed with C57BL/6J males. The research involving animals was conducted in accordance with the Association for Research in Vision and Ophthalmology Statement on the Use of Animals in Ophthalmic and Vision Research and overseen by the Animal Care and Use Committee of the National Eye Institute (Protocol Number NEI-617) under NIH Institutional Biosafety Committee (IBC)-approved Human Pathogen Registration Document (HPRD) #4766 and Recombinant DNA Registration Document RD-09-II-03.

### **Intravitreal injections**

AAV-RS1 vector dilutions of 1E6, 1E7, 5E7, 1E8, 5E8, or 2.5E9 vg/eye or vehicle were administered unilaterally by intravitreal injection (1  $\mu$ l) at postnatal age (PN) 22  $\pm$  3 days (mean  $\pm$  SD) to *Rs1*-KO mice under aseptic conditions. The contralateral eye served as the control and remained untouched. After anesthetizing animals with intraperitoneal ketamine (80 mg  $\cdot$  kg<sup>-1</sup>) and xylazine

(15 mg  $\cdot$  kg<sup>-1</sup>), both eyes of each mouse were dilated with 2.5% phenylephrine hydrochloride (Bausch & Lomb, Inc.) and 0.5% tropicamide (Alcon Laboratories, Inc.). Injected material was sterilized by passage through a 0.22  $\mu$ l filter (Millipore Millex-GS), and the syringes were loaded at the time of injection. Intravitreal injection was performed under a dissecting microscope using a 5  $\mu$ l syringe with a 35-gauge beveled-tip needle (World Precision Instruments, Inc.) inserted through the sclera just posterior to the limbus in the nasal side of the eye. Ocular changes, such as corneal opacity and the amount of reflux from the injection site, were noted for each animal during or immediately after injection. Upon recovery from anesthesia, mice were returned to the animal facility and were monitored daily by the animal husbandry and veterinary staff.

Litters of mice were randomly placed into one of three groups (Table 1): one group was evaluated by ERG, OCT, and RS1 IHC between 3 and 4 months (14  $\pm$  2 weeks) after intravitreal injection of vector (PI); a second group was evaluated by ERG and OCT at 3–4 months PI and was allowed to survive for ERG and IHC evaluation at 6–9 months (31  $\pm$  4 weeks) PI; a third group was evaluated only at the long-term time point (ERG and IHC).

### **Electroretinogram**

The dark-adapted ERG was recorded in both eyes simultaneously to evaluate the efficacy of AAV-RS1 in preserving retinal function at the short-term and long-term time points. The a-wave reflects the activation phase of rod photoreceptors in response to light; the b-wave results from the response of bipolar cells that are activated transsynaptically by photoreceptors. The b-wave-to-a-wave ratio (b/a) normalizes the b-wave by the

**Table 1.** Numbers of mice injected and studied at the short-term and long-term time points

Group	Dose (vg/eye)	No. of mice injected	No. of mice studied <sup>a</sup>				
			3–4 months (14 $\pm$ 2 weeks) postinjection			6–9 months (31 $\pm$ 4 weeks) postinjection	
			ERG	OCT	IHC	ERG <sup>b</sup>	IHC
1	Vehicle	43	41	NA	NA	NA	NA
2	1.0 $\times$ 10 <sup>6</sup>	26	26	16	14	NA	NA
3	1.0 $\times$ 10 <sup>7</sup>	26	26	25	25	NA	NA
4	5.0 $\times$ 10 <sup>7</sup>	26	24	19	13	NA	NA
5	1.0 $\times$ 10 <sup>8</sup>	39	25	20	9	26 (14)	9
6	5.0 $\times$ 10 <sup>8</sup>	41	26	25	12	25 (13)	6
7	2.5 $\times$ 10 <sup>9</sup>	28	27	25	10	17 (0)	15
<b>Total</b>		<b>229</b>	<b>195</b>	<b>130</b>	<b>83</b>	<b>68 (27)</b>	<b>30</b>

ERG, electroretinogram; IHC, immunohistochemistry; OCT, optical coherence tomography.

<sup>a</sup>All but 7 mice survived until their first ERG was recorded at 11–18 weeks or 25–37 weeks. Twenty-five animals died throughout the rest of the study, mostly during or shortly after anesthesia for ERG.

<sup>b</sup>Numbers in parentheses are numbers of animals included in each total that were evaluated only at the long-term time point (e.g., 195 + 27 = 222, the total number of animals that had an ERG done).

photoreceptor response and gives an estimate of effects on the isolated postsynaptic response. The ERG procedure was described previously.<sup>21</sup> Briefly, mice were dark-adapted overnight and all subsequent procedures were performed in dim red light or darkness. After anesthesia and pupil dilation, mice were placed on a heating pad at 37°C and topical anesthesia drops were put in the eye followed by placement of recording electrodes on the cornea. ERG recordings were the average of 1–20 responses to 10  $\mu$ s full-field flashes (Grass Photoc Stimulator PS33; Astro-Med, Inc.) over a range of intensities eliciting threshold through maximum isolated rod responses and mixed rod–cone responses.<sup>24</sup> The intensities to elicit these responses in mouse are similar to those in human. The ERG signals were amplified 5000 times and filtered by a 0.1–1 kHz 3db/decade bandpass and a 60 Hz line filter.

ERG amplitudes in response to the maximum stimulus intensity of 0.6 log cd·s/m<sup>2</sup> were used to evaluate treatment effects. The a-wave was measured from the prestimulus baseline to the maximum value of the negative trough preceding the b-wave. The b-wave amplitude was measured from the a-wave trough to the maximum peak immediately following the a-wave. Oscillatory potentials were not removed before measurement. A-wave time to peak (implicit time) was measured from the time of stimulus onset to the time of the a-wave maximum amplitude. This is also the time of onset of the b-wave originating from postsynaptic activity.

### Optical coherence tomography

The retinas of injected and uninjected eyes were imaged by optical coherence tomography (OCT) at 2–21 days after recording the ERG at the short-term time point when cavities in untreated eyes are maximal in size and distribution<sup>21</sup> using the ultra-high-resolution spectral domain OCT from Bioptigen. This instrument allows noninvasive noncontact imaging of retinal tissue microstructure *in vivo* at 2  $\mu$ m axial resolution. OCT has been used extensively to provide useful structural information in both humans and animal models of retinal degeneration.<sup>25–27</sup>

Mice were anesthetized (80 mg/kg ketamine and 4 mg/kg xylazine) and restrained in a custom holder. They were positioned so that the optic nerve head of the retina was at the center of a rectangular image area of 1.4 mm × 1.4 mm to image 0.7 mm on each side of the optic nerve in the horizontal direction. This area was imaged with 1000 A-scans from the back of the eye to the posterior lens and 100 B-scans across the selected

area. Thus, approximately one-third of the central retina of each mouse was imaged. In addition, images from other areas were regularly obtained to confirm that the central area was representative of the whole retina. Linear B scans were taken in the midretinal horizontal plane through the optic nerve head and 0.6 mm superior and inferior to the optic nerve. The maximum width of “schisis cavities” of treated and untreated *Rs1*-KO retinas was measured using an onscreen micrometer at 4 separate locations along these 3 separate B scans: midpoint on the nasal and temporal side of the optic nerve head and midpoint along the inferior and superior scans (see Supplementary Fig. S1; Supplementary Data are available online at [www.liebertpub.com/hum](http://www.liebertpub.com/hum)). Raw measurements were graded: 1, no cavities; 2, <30  $\mu$ m; 3, 30–49  $\mu$ m; 4, 50–69; 5, 70–99; 6,  $\geq$ 100. The grades were combined to generate a score for each retina: final score = (minimum at position 1–4 + maximum at position 1–4)/2. Using categories and assigning a value of 1 if no cavities were present avoided division by zero in calculating the ratio of treated-to-untreated eye (see Statistical procedures section below). Outer nuclear layer (ONL) thickness was measured at 500  $\mu$ m from the optic nerve in the nasal and temporal retina. The two measurements were averaged to give a single value for each retina. The identity of the samples was masked at the time of measurement.

### RS1 protein immunohistochemistry

Retinas were processed for RS1 protein IHC at the 14- or 31-week PI time point. From 1 to 21 days after the ERG or OCT, the mice were euthanized and perfused with 4% paraformaldehyde in sodium phosphate buffer. The eyes were removed and fixed overnight in 4% paraformaldehyde and 0.5% glutaraldehyde in sodium phosphate buffer followed by processing for cryosectioning. Twenty-five sagittal sections of the injected eye were taken beginning at the nasal margin of the retina and proceeding through and including the optic nerve head and approximately 200  $\mu$ m of the temporal retina. The sections were stained using a rabbit polyclonal antibody against the N-terminus of retinoschisin (amino acid residues 24–37) and a secondary antibody conjugated to red-fluorescent Alexa Fluor 568 dye (Invitrogen). Nuclei were stained with DAPI.

Retinoschisin expression in retinas of eyes receiving AAV-RS1 and untreated eyes was visually evaluated using a Nikon E800 fluorescence microscope to determine the intensity and extent of immunostaining in four vertical sections taken at evenly spaced intervals from the nasal margin of

the retina to the optic nerve head and one section taken temporal to the optic nerve. The results from these five sections were averaged. In each section from a vector-treated *Rs1*-KO retina, stain intensity in the photoreceptor and inner retinal layers was subjectively graded on a scale from 0 to 4 relative to a WT C57BL/6J mouse retina (grade = 4.0), which was stained at the same time to help control for variations in the level of background staining with each batch. Grade increased with both brightness and the spread of staining from the photoreceptor inner segments, where it was first detected, to the inner retina (Supplementary Fig. S2A). Because retinoschisin staining was not uniformly distributed across the sections from most treated retinas, the weakest and strongest intensities in each section were graded and these were added together and multiplied by the proportion of the section showing at least minimum staining to obtain a single score for each retina ( $[\text{minimum grade} + \text{maximum grade}] \times [\text{proportion of section stained}]$ ) (Supplementary Fig. S2B). Thus, WT retinas received a score of 8 ( $[4 + 4] \times 1$ ). Though time- and labor-intensive, this method allowed visualization of the distribution of protein within the layers and along the retinal length. The scoring of all retinas was done by a single experienced observer (Y.Z.) and the identity of the section was masked at the time of analysis. Values are reported as staining score and compared across doses using nonparametric statistics (see below). A similar subjective scoring of the intensity and extent of GFP fluorescence viewed by indirect ophthalmoscopy in nonhuman primate retina was used to compare expression efficiency of different vectors and doses.<sup>28</sup>

### Statistical procedures

ERG amplitude and OCT results were evaluated by calculating the ratio of the treated eye to the untreated eye (T/UT) in each mouse and averaging these values for each dose. The difference between the two eyes was used for the a-wave implicit time (UT-T) and ONL thickness (T-UT) instead of the ratio. This helped control for variability between animals and allowed direct comparison of outcomes to the vehicle-treated group (ERG only) and across treatment groups using the one-way ANOVA and multiple comparison tests (parametric with Bonferroni's test for ERG and ONL and nonparametric Kruskal–Wallis test with Dunn's test for OCT). Outliers in the T/UT values for each dose were removed using the ROUT method<sup>29</sup> before statistical analysis. For retinoschisin IHC, the average raw score for treated eyes in each group was calculated

and the Kruskal–Wallis nonparametric one-way ANOVA with Dunn's multiple comparison test was used to compare between groups. Where indicated, the one-sample *t*-test was performed when comparing each dose to the theoretical “no effect” level of 1 for T/UT (ERG and cavities) or 0 for UT-T (a-wave implicit time), T-UT (ONL thickness), and retinoschisin staining score. Values are shown as mean  $\pm$  SEM. Paired *t*-tests were also performed on raw ERG amplitudes and OCT data for each dose, and all measurements were included in this analysis (Supplementary Fig. S3). All statistics were performed using GraphPad Prism version 6.05 for Windows (GraphPad Software).

## RESULTS

### Retinal function and structure was improved, and widespread RS1 staining was seen in *Rs1*-KO retinas treated with AAV-RS1

The ERG, OCT, and IHC results from an *Rs1*-KO mouse treated in one eye with 2.5E9 vg/eye AAV-RS1 and a WT mouse are shown in Fig. 1. As previously shown,<sup>20,21,30</sup> the b-wave in the untreated eye is disproportionately reduced compared with the a-wave, which results in a reduced b-wave-to-a-wave amplitude (b/a) ratio compared with WT type. The fellow eye treated with AAV-RS1, however, has a substantially larger b-wave amplitude and b/a ratio. In OCT images, the untreated eye has widely distributed large cavities, which increase overall retinal thickness compared with WT, but measurable cavities are absent from the treated eye (cavity score = 1). RS1 protein IHC staining in Fig. 1 shows that the AAV-RS1-treated retina received an RS1 staining score approximately one-half that of WT. The staining is strongest in the photoreceptor inner segments of both the WT and treated *Rs1*-KO retinas, whereas the untreated retina of the *Rs1*-KO mouse shows only nonspecific background staining.

### Retinal function and structure show the same response to vector dose

*Rs1*-KO mice were administered AAV-RS1 at doses ranging from 1E6 to 2.5E9 vg/eye and analyzed by ERG at 3–4 months PI. All three ERG amplitude parameters (a-wave and b-wave amplitude and b/a ratio) indicated that the lowest dose that resulted in a significantly higher treated-to-untreated eye ratio (T/UT) when compared with vehicle was 1E8 vg/eye ( $p < 0.01$ – $0.0001$ ; Fig. 2). Doses from 1E6 to 5E7 vg/eye were not significantly more effective than vehicle. The b-wave at the threshold dose was more than 2-fold higher in the

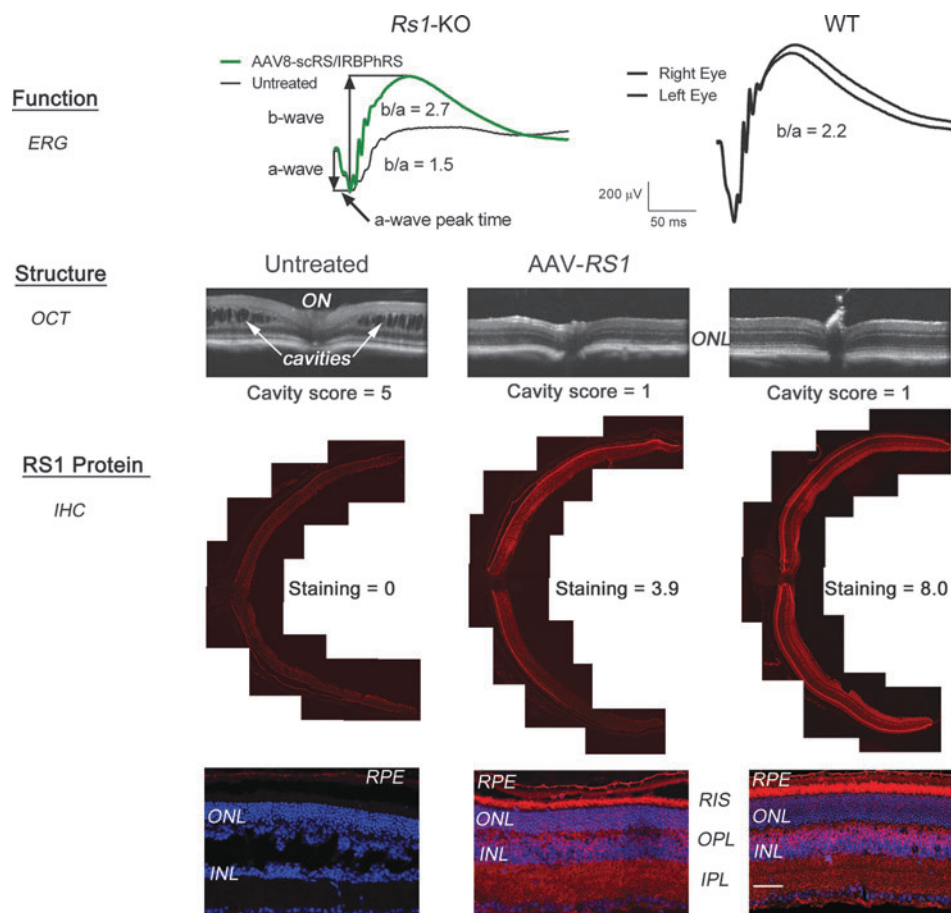


**Figure 1.** Retinal function, structure, and RS1 protein expression in an *Rs1*-KO mouse treated in one eye with 2.5E9 vg/eye AAV-RS1 by intravitreal injection and in a wild-type (WT) mouse. Function was monitored with the electroretinogram (ERG) a-wave and b-wave amplitude, the ratio of the b-wave-to-the a-wave amplitude (b/a), and the a-wave implicit time (time to peak) recorded 14 weeks postinjection (PI). In the untreated eye of the *Rs1*-KO mouse, the b-wave was reduced much more than the a-wave, resulting in a reduced b/a ratio compared with WT. In the fellow treated eye, the b-wave had a much larger amplitude without much change in the a-wave, resulting in increased b/a ratio. Optical coherence tomography (OCT) was used to view retinal structure *in vivo*. Each image shows 1.4 mm of the central retina (about 1/3 the total retinal length) including the optic nerve (ON). Images are oriented with vitreal side up. The untreated eye has large cavities spanning the layers proximal to the photoreceptor nuclear layer (ONL). Cavity size at 4 positions along 3 retinal scans in each retina was graded from 1 to 6 to obtain a score. A score of 1=no cavities. Treated eyes show an absence of measurable cavities and overall better organization of retinal lamina and thicker ONL. RS1 protein staining was evaluated in the *Rs1*-KO animal at 27 weeks PI and in an age-matched WT mouse by immunohistochemistry (red). Retinas were visually graded for intensity and distribution on a scale relative to WT (see Methods). No RS1 protein was detected in untreated eyes. Fewer cavities are seen in this section than in OCT because, as described in the text, cavity size peaks at about 4 months PN and spontaneously declines at later ages. In the treated retina, staining was close to 50% of WT and was distributed along most of the retinal length. Higher-magnification confocal images from retinas of another *Rs1*-KO mouse treated with the same dose of AAV-RS1 show that protein distribution across the retinal layers is similar to that seen in WT. This mouse was analyzed at 14 week PI, and the untreated eye still shows large cavities between the nuclear layers stained with DAPI (blue). INL, inner nuclear layer; IPL, inner plexiform layer; ONL, outer nuclear layer; OPL, outer plexiform layer; RIS, rod inner segments; scale bar = 50  $\mu$ m.

treated eye than in the untreated eye, whereas the a-wave and b/a ratio were 1.4- and 1.5-fold higher, respectively. All doses >1E8 vg/eye also produced significant improvement except for the a-wave at 5E8 vg/eye, but there was no significant increase in effect beyond that seen with the threshold dose of 1E8 vg/eye. In addition, the reduction in the a-wave implicit time in treated compared with untreated eyes (UT-T) was significant compared with vehicle at doses of 1E8 vg/eye and higher (Fig. 2). Unlike amplitude, this effect was significantly greater at 2.5E9 vg/eye ( $p < 0.001$ ) than at threshold.

AAV-RS1 treatment with the same six vector doses was evaluated for its effect on inner and outer retinal morphology by OCT imaging of retinal cavities and ONL thickness *in vivo* and calculating T/UT for cavity size and T-UT for ONL (Fig. 3). Like the ERG, 1E8 vg/eye was the lowest dose that produced a significant effect (cavities,  $p < 0.0001$ ; ONL,  $p < 0.01$ ), and the three highest doses were statistically equivalent to each other. As vehicle-injected eyes were not evaluated by OCT, this analysis was based on comparison to 1E6 vg/eye, which was not significantly different from the the-

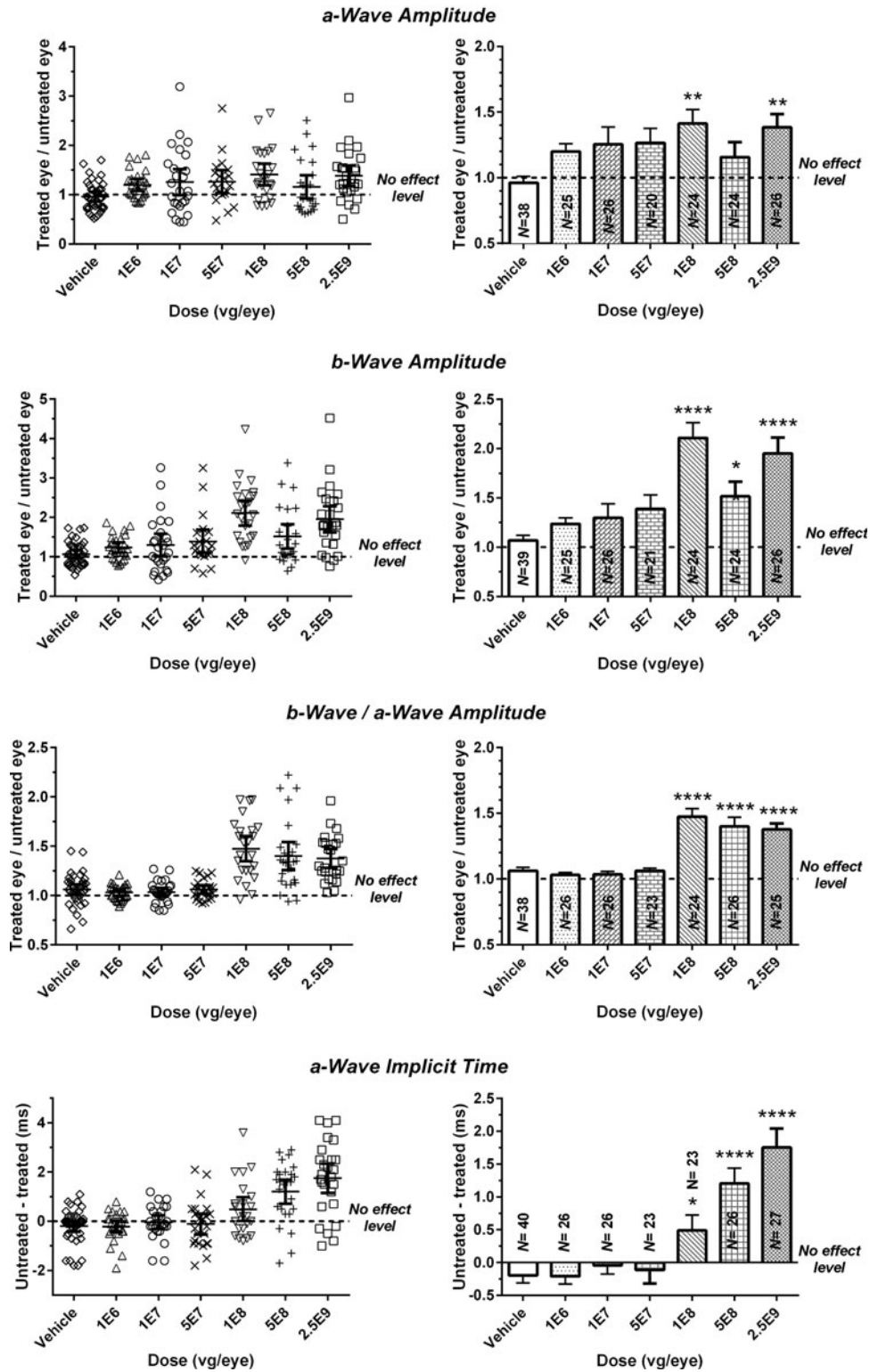


**Figure 2.** ERG dose response of *Rs1*-KO mice treated in one eye with AAV-*RS1* or vehicle at 22±3 days PN and evaluated at 14±2 weeks after intravitreal injection. The ratio of the treated eye to the untreated eye (T/UT) is plotted for the a-wave amplitude, b-wave amplitude, and b-wave/a-wave amplitude. The untreated eye minus the treated eye (UT-T) is plotted for the a-wave implicit time. The scatter plots show the results from individual mice at each dose, and the bar graphs show the averages and SEM for each dose. A value of 1 represents no effect for the amplitude parameters and 0 represents no effect for the a-wave implicit time. Asterisks indicate significance of treatment effect compared with vehicle (\*\*\*\**p*<0.0001, \*\**p*<0.01, \**p*<0.05).

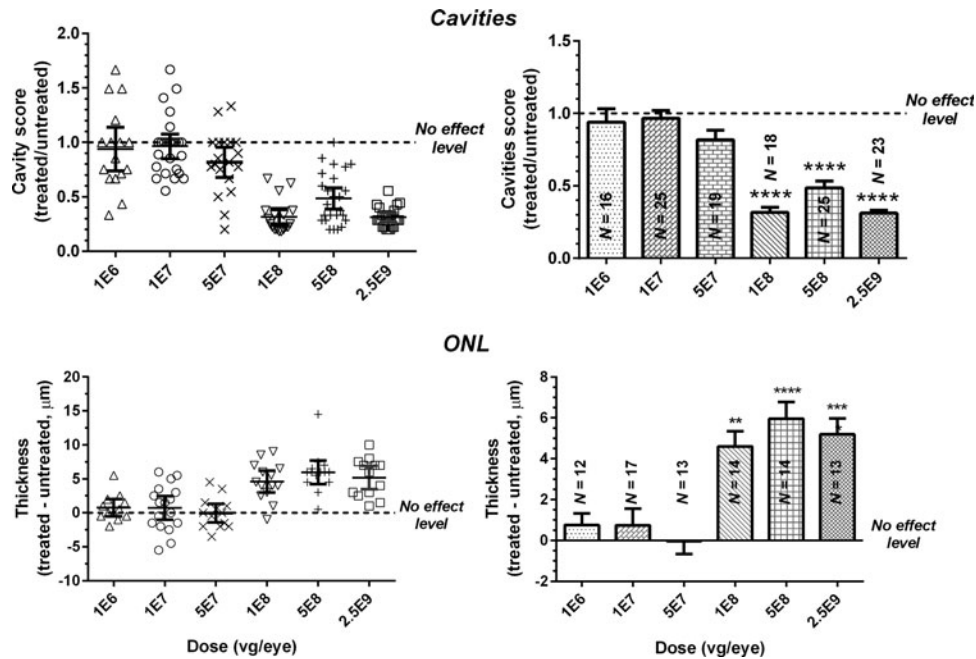


**Figure 3.** Dose response of retinal cavity score and ONL thickness in *Rs1*-KO mice treated in one eye with AAV-RS1 by intravitreal injection. Retinas were viewed *in vivo* using OCT after the ERG at  $14 \pm 2$  weeks postinjection. Cavity size in each retina was scored by width, and ONL thickness was measured as described in the Methods. Treated divided by untreated eye (T/UT) is plotted for cavities, and treated eye minus untreated eye (T-UT) is plotted for ONL thickness. The scatter plots show the T/UT or T-UT values for individual mice in each dose group, and the bar graph shows the average and SEM. Asterisks indicate significance of the effect compared with 1E6 vg/eye. Cavities: Kruskal–Wallis test, Dunn’s multiple comparison test. ONL: ordinary one-way ANOVA, Holm–Sidak’s multiple comparison test. \*\* $p < 0.001$ , \*\*\* $p < 0.001$ , \*\*\*\* $p < 0.0001$ .

oretical no-effect level of 1 (cavities:  $T/U = 0.94 \pm 0.09$  SEM) or 0 [ONL:  $T-UT = -0.75 \pm 0.6 \mu\text{m}$ , one-sample *t*-test). Comparison of raw data from treated and untreated eyes in each mouse using the paired *t*-test (Supplementary Fig. S3) indicated a threshold of 5E7 vg/eye for improvement in the a-wave and b-wave amplitude ( $p < 0.05$ ) and cavity size ( $p < 0.01$ ), though the effect was much smaller than at 1E8 vg/eye. The threshold for the b/a ratio and ONL thickness was 1E8 vg/eye ( $p < 0.0001$ ).

### RS1 IHC staining showed dose dependence over a larger range of doses than structure and function

Immunohistochemical staining of RS1 in AAV-RS1-treated retinas increased with increased vector dose (Fig. 4A). Subjective grading of stain intensity and distribution using criteria described in the Methods indicated a statistically significant dose response ( $p < 0.0001$ , nonparametric one-way ANOVA). No specific staining of retinal layers (staining score = 0) was observed in untreated eyes. Only 1E6 vg/eye did not produce significant staining above zero (one-sample *t*-test); therefore, this was used as baseline for comparison across doses. Doses of 5E7 vg/eye ( $p < 0.05$ ), 1E8, 5E8, and 2.5E9 vg/eye ( $p < 0.0001$ ) showed significant levels of

staining compared with 1E6 vg/eye. Unlike ERG and OCT, staining continued to increase above threshold. To further characterize this increase, the Michaelis–Menten equation was fit to the log vector dose versus staining data (Fig. 4A). The fit obtained over the entire range of doses (1E6–2.5E9 vg/eye) had an  $R^2$  of 0.64. The  $K_m$ , or dose giving  $\frac{1}{2}$  the maximum response, was 1.0E8 vg/eye, with the maximum response ( $V_{max}$ ) being 4.0, much less than WT staining (8.0).

### Structural and functional improvement and RS1 staining was maintained at 6–9 months after treatment

RS1 staining and efficacy were monitored for doses of 1E8, 5E8, and 2.5E9 vg/eye at 6–9 months PI. The RS1 staining score tended to be higher than at the short-term time point (Fig. 4B), but the difference between the two time points was only significant at 1E8 vg/eye ( $p < 0.05$ ). This level continued to be associated with functional and structural efficacy. The a-wave and b-wave amplitudes and the b/a ratio remained significantly larger than that in untreated fellow eyes ( $T/UT > 1$ ; Fig. 5). The effect on the a-wave was significantly greater at 6–9 months PI than at 3–4 months PI at 5E8 vg/eye ( $p < 0.01$ ) and on the b-wave at 1E8 vg/eye ( $p < 0.05$ ), but was

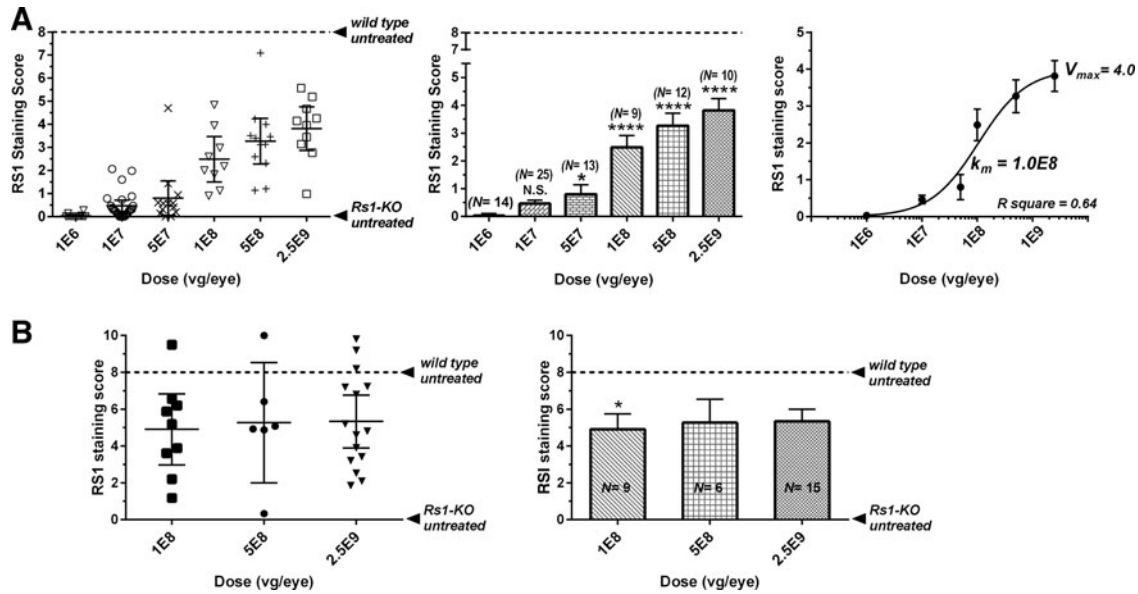


**Figure 4.** Retinoschisin protein (RS1) immunohistochemistry staining scores (see Methods) in retinas of *Rs1*-KO mice treated with AAV-RS1 in one eye. Immunohistochemistry was done after OCT evaluation and/or ERG recordings. **(A)** RS1 staining score in treated eyes versus vector dose at 14±2 weeks after intravitreal injection: scatter plot of data from individual mice, average by dose, and Michaelis–Menten equation ( $Y = V_{max} \frac{X}{K_m + X}$ ) fit to the average data from 1E6–2.5E9 vg/eye ( $K_m = 1.0E8$ ,  $V_{max} = 4.0$ ). Asterisks indicate a significant difference between each dose and 1E6 vg/eye. **(B)** Dose response for RS1 staining in retinas from eyes of *Rs1*-KO mice injected with 1E8, 5E8, or 2.5E9 vg/eye and evaluated after the ERG recording at 31±4 weeks after injection. Asterisks indicate a significant difference from the same dose at the early time point **(A)**. *p*-Values were calculated using the nonparametric one-way ANOVA (Kruskal–Wallis test) and Dunn’s multiple comparison test (\* $p < 0.05$ , \*\*\*\* $p < 0.0001$ ).

not different at the other two doses. The treatment effect on the b/a ratio, however, was less than it was at the early time point for 1E8 and 5E9 vg/eye ( $p < 0.001$ ), probably due, in part, to the natural history of changes in untreated eyes (see Discussion). The a-wave implicit time (b-wave latency) was still significantly faster in treated eyes (UT-T > 0) at 6–9 months except at 1E8 vg/eye, which showed a significant ( $p < 0.05$ ) decline in UT-T compared with the early time point. Cavities were not evaluated at the long-term time point because of the previously reported spontaneous decline in cavities in untreated *RS1*-KO mice beyond 4 months of age.<sup>21</sup>

## DISCUSSION

AAV-RS1 vector administered by a single intravitreal injection in the experimental XLRs model, *Rs1*-KO mouse, produced significant improvement in retinal structure, indicated by a reduction in cavities and increased ONL. Improved function was shown by an increase in b-wave and a-wave amplitude and b/a ratio and a decrease in the a-wave implicit time. The threshold dose for all measures was 1E8 vg/eye. Doses one-half log lower did not show efficacy, and doses above threshold did not have an effect significantly different from threshold (except for ERG timing at 2.5E9 vg/eye). IHC staining for the

RS1 protein in the retina also increased with dose, though it increased more gradually than the step-like dose response of structure and function. IHC also indicated that structural and functional efficacy occurred when protein staining was much less than in WT retinas, suggesting that efficacy does not require RS1 expression at the level of WT.

Protein staining remained stable or was increased by 6–9 months compared with 3–4 months, as were a-wave and b-wave amplitudes in treated eyes relative to untreated eyes. Amplitude data indicated that there was some decline in treated eyes between the two time points (Supplementary Fig. S3 and S4) but much less than in untreated eyes. Previously, we have shown that *Rs1*-KO mice maintain RS1 staining and significantly larger b-wave amplitudes 14 months after intravitreal treatment with AAV-Rs1. The improvement in b/a ratio for doses 1e8 and 5e8 vg/eye was reduced at 6–9 months compared with 3–4 months. The natural history of the untreated *RS1*-KO mouse phenotype shows a spontaneous decrease in the cavity number and size and an increase in b/a ratio beginning between 4 and 6 months PN.<sup>21</sup> This reduces the relative effect of treatment when T/UT is calculated. In addition, the effect of treatment in slowing photoreceptor loss, and hence slowing the a-wave reduction with age, is more apparent over

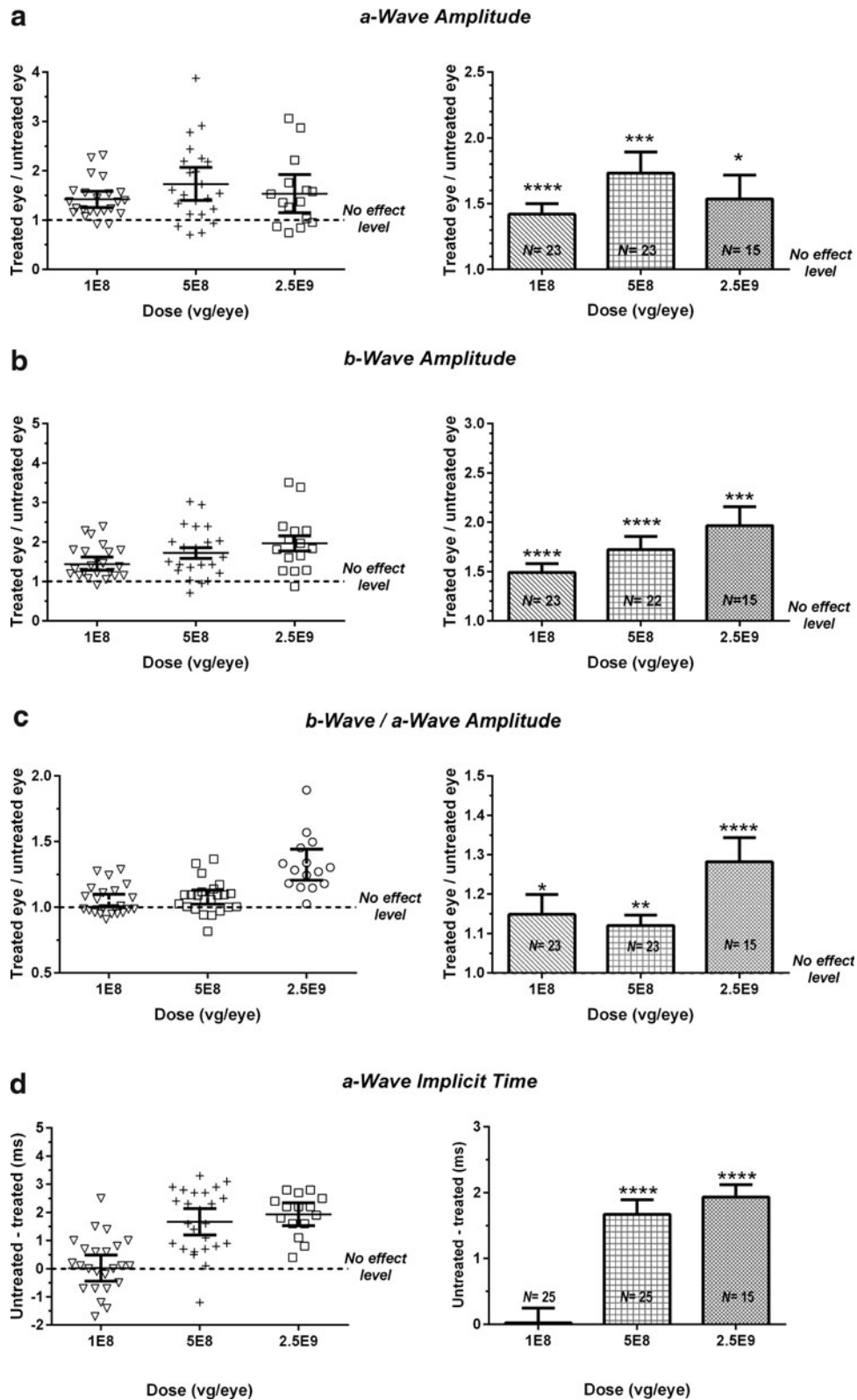


**Figure 5.** Long-term effects of treatment with AAV-RS1 on retinal function. The ERG was recorded  $31 \pm 4$  weeks after intravitreal injection in one eye of *Rsl-KO* mice at  $22 \pm 3$  days PN. Treated/untreated eye is plotted for a-wave and b-wave amplitude and b/a ratio. The a-wave implicit time is plotted as the untreated minus treated eye. Asterisks indicate a significant difference from the hypothetical no-effect level of 1 for the amplitude and 0 for the a-wave timing. One-sample *t*-test; \* $p < 0.05$ , \*\* $p < 0.01$ , \*\*\* $p < 0.001$ , \*\*\*\* $p < 0.0001$ .

the longer term, and contributes to reducing the b/a ratio in treated eyes.

### Mechanism of therapeutic effect

The XLRS and *Rs1*-KO phenotypes result from loss of retinoschisin function. The protein that is expressed in photoreceptors and bipolar cells of the mouse<sup>12,14</sup> and human<sup>12</sup> retina is absent in *Rs1*-KO mice,<sup>19,20</sup> and in a subset of XLRS patients with the most severe mutations.<sup>10</sup> The therapeutic effect in *Rs1*-KO mice is linked to replacement of the missing protein with its human homolog. Use of the native promoter and the tropism of AAV8 ensured that the retinal distribution of RS1 was indistinguishable from the WT mouse retina in our IHC sections (Fig. 1 and Supplementary Fig. S2), which presumably is most effective at restoring RS1 function in the retina. Byrne et al.<sup>31</sup> showed, however, that widespread RS1 distribution can also be produced when gene delivery is targeted to Müller glial cells using a cell-specific AAV6 variant, ShH10, with a ubiquitous promoter. In addition, targeting expression to photoreceptors using the AAV2 variant 7m8 and a rhodopsin promoter produced a protein distribution pattern similar to WT and the most effective long-term rescue. Thus, for this secreted protein, it may not be necessary to produce a strictly WT pattern of cellular expression to achieve efficacy, though targeting cell types using the proper promoter and vector is important for optimal success of gene therapy.<sup>30</sup> In our analysis of the dose response of IHC staining for retinoschisin, we observed that staining first saturated in the photoreceptor inner segments before spreading to the inner retina to produce a more WT-like expression pattern at higher doses (Supplementary Fig. S2A). This spread was associated with structural and functional efficacy, again suggesting that a normal distribution pattern by targeting specific cell types is important for therapeutic effect. An additional reason for using an *RS1* promoter is that it should eliminate off-target expression in the eye<sup>32</sup> and elsewhere and reduce toxicity.

Retinal cavities are primarily found in the synaptic layer between photoreceptors and bipolar cells in the *Rs1*-KO mouse, and our results suggest that this structural pathology is ameliorated when vector dose is high enough to produce significant levels of protein in this layer. We noted that the ERG a-wave, b-wave, and b/a ratio were all increased relative to untreated eyes at the dose producing significant reduction in cavities. The implication is that reduction in cavities in the synaptic layer with AAV-RS1 treatment enhances synaptic processing and/or function of postsynaptic cells.<sup>17,18</sup> The

b-wave originates from extracellular currents generated primarily by bipolar cells postsynaptic to photoreceptors.<sup>33,34</sup> Thus, increased b-wave amplitude in treated eyes is consistent with improved postsynaptic responses. On the other hand, the a-wave and ONL thickness were increased, indicating an improvement in photoreceptor number and responses generated by outer segment currents, which could result in increased signaling to bipolar cells. Previous longer-term studies also showed a substantial difference in photoreceptor number and organization between treated and untreated eyes.<sup>21,35</sup> The fact that treatment improved the b-wave proportionally more than the a-wave (b/a ratio treated > b/a ratio untreated) indicates that the postsynaptic response was not entirely because of the improvement of photoreceptor responses. This is consistent with structural changes in the OPL and INL resulting in improved postsynaptic responses.

Previously, we reported that treatment with AAV-RS1 restored postsynaptic signaling protein distribution in the dendritic tips and the resting membrane potential of bipolar cells in *Rs1*-KO mice to normal.<sup>17</sup> We also reported that changes in levels of synaptic proteins with age in the *Rs1*-KO mouse are mirrored by changes in the ERG b-wave and b/a ratio, though a direct link was not demonstrated.<sup>18</sup> In the current study, we noted that the a-wave implicit time, which is also the onset or latency of the postsynaptic b-wave, had the same threshold for efficacy as the amplitude changes, but had a more graded dose response similar to IHC staining for RS1. This suggests a direct effect of RS1 on the structural integrity of the postsynaptic layer that enhances the speed and/or strength of synaptic processing. We previously provided evidence that phototransduction is not altered in adult *Rs1*-KO mice,<sup>36</sup> thus supporting the idea that changes we see in the a-wave implicit time are related to either pre- or postsynaptic processing. The ERG, however, is a combination of overlapping extracellular retinal potentials, which may interact to influence the timing of response peaks. Thus, the direct effect on synaptic function should be confirmed with cellular recordings.

### Treatment age

Mice in this study were treated at an average age of 22 days, by which time the retina is structurally mature. This corresponds to the beginning of the period of most rapid progression of the phenotype in mice.<sup>21</sup> There is a delay, however, in achieving therapeutic levels of RS1 protein. In an unpublished study of the time course of IHC staining of RS1 from 1 to 15 weeks PI ( $n=6-16$  animals

per time point; Zeng, unpublished data), we found that, on average, AAV-RS1 at 2.5E9 vg/eye produced a significant increase above baseline as early as 1 week PI. Average staining score, however, only reached levels associated with efficacy between 4 and 6 weeks after intravitreal injection, although a few animals had therapeutic levels at all earlier time points. This would suggest that therapeutic levels of the RS1 protein in animals in the current efficacy study were reached no earlier than about 7 weeks of age when the *Rs1*-KO phenotype is well advanced.<sup>21</sup> As cavities are almost completely absent and the ERG b/a ratio is in the normal range in many treated retinas by 3–4 months PI (e.g., Fig. 1), it is reasonable to assume that there is a reversal of the structural and functional changes, as opposed to prevention or slowing of progression. Together with our earliest work showing effective treatment of adult mice,<sup>20</sup> this study supports the possibility of an effective treatment by this vector and route of administration in adult humans. In addition, we have shown therapeutic effect on the ERG and retinal structure by OCT in mice injected at 6 months of age and older (Zeng, unpublished).

There are several reasons for selecting an age of 3 weeks for intravitreal treatment. Our natural history study showed that the structural and functional parameters of the phenotype (cavity size and ERG b/a ratio) begin to spontaneously return toward normal between 4 and 6 months in mice.<sup>21</sup> So, in addition to the fact that it takes some time for protein expression to occur at a substantial level, we thought that it is advisable to dose at a young age to allow sufficient time for therapeutic action of the protein to manifest before these spontaneous changes. In human XLRS, progressive decline in b-wave amplitude and b/a ratio occurs between 4.5 and 55 years, as seen in a recent cross-sectional analysis of 68 XLRS patients with “noticeably severe” mutations.<sup>10</sup> The data indicated that most patients between 20 and 30 years had the lowest b/a ratio values for the population. In terms of the disease phenotype, this may correspond to the period of most rapid progression in *Rs1*-KO mice between 1 and 4 months PN since it is roughly equivalent to 3–6 months of age in mice. Thus, efficacy was tested during a period of rapid disease progression that simulates the time course for the majority of XLRS patients with severe disease and also roughly corresponds to the same developmental age in humans.

#### Translation of dosing efficacy to human

In addition to demonstrating proof-of-concept that delivery of AAV-RS1 into the vitreous of the

eye can reduce retinal cavities and improve retinal function, this study provides guidance in dose selection for human XLRS patients in the clinical trial. Translating the efficacious dose in the mouse to equivalency in humans, however, is not straight forward, as it is not known which factor is most important in predicting how many vector particles reach the target cells. Vitreal volume would be relevant for calculating the dilution in the eye but not necessarily the dose reaching the retina. Differences in the physiology of the vitreous between mouse and human<sup>37</sup> and the geometry of the injection, including distance from the retina, suggest that the difference in vitreal volume (approximately 1000-fold) is an underestimation of the scaling factor. If the majority of vector injected into the vitreous is delivered to the retinal surface in mouse and human, then retinal surface area, approximately a 70-fold difference,<sup>38,39</sup> or number of transduced cells, a 10-fold difference for photoreceptors,<sup>38,40</sup> is a possible factor. This 100-fold range is reflected in dose-escalation range of our clinical trial (NCT02317887). Vector penetration of the retina from the vitreous leading to transduction in mice depends on the presence of the retinoschisis phenotype; our clinical vector readily penetrates the retina in the *Rs1*-KO mouse, but there is much less penetration in WT mice.<sup>32</sup> It is unknown how penetration in the human retinoschisis eye compares to the mouse *Rs1*-KO eye. In addition to the wide range of scale-up factors to consider, this complicates an accurate estimation of the dose necessary to transduce, express, and result in efficacy in the human eye. For this reason, the phase I/II clinical investigation is designed as dose-escalation study with the intent to identify a dose that is safe and provides biological activity.

Additional studies delivering our clinical vector by the vitreal or subretinal route to the nonhuman primate (NHP) retina are being considered to test its ability to elicit expression in primate photoreceptors, which is important for efficacy,<sup>31</sup> as well as other cell types. Our AAV-RS1 vector consists of the human promoter and coding sequence, thus giving it the best chance of being expressed in humans with XLRS. In addition, it is known that AAV8 efficiently transduces canine<sup>41</sup> and NHP<sup>28</sup> photoreceptors when delivered by subretinal injection. Testing expression of our vector–promoter construct in NHP would require using GFP or a tagged RS1 to distinguish it from native protein. Peptide tags, including a 9-amino-acid myc and FLAG epitope, were used in studies of RS1 *in vitro*<sup>42,43</sup> or in the *Rs1*-KO mouse (Vijayasarathy, unpublished) and found not to

interfere with normal expression, cellular localization, secretion, and, in the latter case, retinal function and rescue. These tags are small enough to be incorporated into our transgene in the scAAV8 vector and would allow meaningful testing of the clinical construct in NHP.

## ACKNOWLEDGMENTS

This study was supported by the intramural research program of the National Institute on Deaf-

ness and Other Communication Disorders, the National Eye Institute, and the National Institutes of Health. We would like to acknowledge Dr. Lisa Wei for helpful comments on the manuscript.

## AUTHOR DISCLOSURE

Peter Colosi works on development of gene therapy products at BioMarin Pharmaceutical. No other authors have competing financial interests.

## REFERENCES

- Bainbridge JW, Smith AJ, Barker SS, et al. Effect of gene therapy on visual function in Leber's congenital amaurosis. *N Engl J Med* 2008;358:2231–2239.
- Bennicelli J, Wright JF, Komaromy A, et al. Reversal of blindness in animal models of leber congenital amaurosis using optimized AAV2-mediated gene transfer. *Mol Ther* 2008;16:458–465.
- Cideciyan AV, Aleman TS, Boye SL, et al. Human gene therapy for RPE65 isomerase deficiency activates the retinoid cycle of vision but with slow rod kinetics. *Proc Natl Acad Sci U S A* 2008;105:15112–15117.
- Cideciyan AV, Hauswirth WW, Aleman TS, et al. Human RPE65 gene therapy for Leber congenital amaurosis: Persistence of early visual improvements and safety at 1 year. *Hum Gene Ther* 2009;20:999–1004.
- Cideciyan AV, Hauswirth WW, Aleman TS, et al. Vision 1 year after gene therapy for Leber's congenital amaurosis. *N Engl J Med* 2009;361:725–727.
- Maguire AM, High KA, Auricchio A, et al. Age-dependent effects of RPE65 gene therapy for Leber's congenital amaurosis: A phase 1 dose-escalation trial. *Lancet* 2009;374:1597–1605.
- Pierce EA, Bennett J. The status of RPE65 gene therapy trials: Safety and efficacy. *Cold Spring Harb Perspect Med* 2015;5:a017285.
- Molday RS, Kellner U, Weber BH. X-linked juvenile retinoschisis: Clinical diagnosis, genetic analysis, and molecular mechanisms. *Prog Retin Eye Res* 2012;31:195–212.
- Prenner JL, Capone A Jr., Ciaccia S, et al. Congenital X-linked retinoschisis classification system. *Retina* 2006;26:S61–S64.
- Bowles K, Cukras C, Turriff A, et al. X-linked retinoschisis: *RS1* mutation severity and age affect the ERG phenotype in a cohort of 68 affected male subjects. *Invest Ophthalmol Vis Sci* 2011;52:9250–9256.
- Grayson C, Reid SN, Ellis JA, et al. Retinoschisin, the X-linked retinoschisis protein, is a secreted photoreceptor protein, and is expressed and released by Weri-Rb1 cells. *Hum Mol Genet* 2000;9:1873–1879.
- Molday LL, Hicks D, Sauer CG, et al. Expression of X-linked retinoschisis protein RS1 in photoreceptor and bipolar cells. *Invest Ophthalmol Vis Sci* 2001;42:816–825.
- Reid SN, Akhmedov NB, Piriev NI, et al. The mouse X-linked juvenile retinoschisis cDNA: Expression in photoreceptors. *Gene* 1999;227:257–266.
- Takada Y, Fariss RN, Tanikawa A, et al. A retinal neuronal developmental wave of retinoschisin expression begins in ganglion cells during layer formation. *Invest Ophthalmol Vis Sci* 2004;45:3302–3312.
- Sauer CG, Gehrig A, Warneke-Wittstock R, et al. Positional cloning of the gene associated with X-linked juvenile retinoschisis. *Nat Genet* 1997;17:164–170.
- Vogel WF, Abdulhussein R, Ford CE. Sensing extracellular matrix: An update on discoidin domain receptor function. *Cell Signal* 2006;18:1108–1116.
- Ou J, Vijayasaraty C, Ziccardi L, et al. Synaptic pathology and therapeutic repair in adult retinoschisis mouse by AAV-*RS1* transfer. *J Clin Invest* 2015;125:2891–2903.
- Takada Y, Vijayasaraty C, Zeng Y, et al. Synaptic pathology in retinoschisis knockout (*Rs1<sup>-/-</sup>*) mouse retina and modification by rAAV-*Rs1* gene delivery. *Invest Ophthalmol Vis Sci* 2008;49:3677–3686.
- Weber BH, Schrewe H, Molday LL, et al. Inactivation of the murine X-linked juvenile retinoschisis gene, *Rs1h*, suggests a role of retinoschisin in retinal cell layer organization and synaptic structure. *Proc Natl Acad Sci U S A* 2002;99:6222–6227.
- Zeng Y, Takada Y, Kjellstrom S, et al. *RS-1* gene delivery to an adult *Rs1h* knockout mouse model restores ERG b-wave with reversal of the electronegative waveform of X-linked retinoschisis. *Invest Ophthalmol Vis Sci* 2004;45:3279–3285.
- Kjellstrom S, Bush RA, Zeng Y, et al. Retinoschisin gene therapy and natural history in the *Rs1h*-KO mouse: Long-term rescue from retinal degeneration. *Invest Ophthalmol Vis Sci* 2007;48:3837–3845.
- U.S. Food and Drug Administration, Center for Biologics Evaluation and Research (2013) Pre-clinical Assessment of Investigational Cellular and Gene Therapy Products.
- Marangoni D, Wu Z, Wiley HE, et al. Preclinical safety evaluation of a recombinant AAV8 vector for X-linked retinoschisis after intravitreal administration in rabbits. *Hum Gene Ther Clin Dev* 2014;25:202–211.
- Marmor MF, Fulton AB, Holder GE, et al. ISCEV Standard for full-field clinical electroretinography (2008 update). *Doc Ophthalmol* 2009;118:69–77.
- Cuenca N, Fernandez-Sanchez L, Sauve Y, et al. Correlation between SD-OCT, immunocytochemistry and functional findings in an animal model of retinal degeneration. *Front Neuroanat* 2014;8:151.
- Gerth C, Zawadzki RJ, Werner JS, et al. Retinal morphological changes of patients with x-linked retinoschisis evaluated by fourier-domain optical coherence tomography. *Arch Ophthalmol* 2008;126:807–811.
- Schaal KB, Freund KB, Litts KM, et al. Outer retinal tubulation in advanced age-related macular degeneration: Optical coherence tomographic findings correspond to histology. *Retina* 2015;35:1339–1350.
- Vandenberghe LH, Bell P, Maguire AM, et al. Dosage thresholds for AAV2 and AAV8 photoreceptor gene therapy in monkey. *Sci Transl Med* 2011;3:88ra54.
- Motulsky HJ, Brown RE. Detecting outliers when fitting data with nonlinear regression—A new method based on robust nonlinear regression and the false discovery rate. *BMC Bioinform* 2006;7:123.
- Min SH, Molday LL, Seeliger MW, et al. Prolonged recovery of retinal structure/function after gene therapy in an *Rs1h*-deficient mouse model of x-linked juvenile retinoschisis. *Mol Ther* 2005;12:644–651.
- Byrne LC, Ozturk BE, Lee T, et al. Retinoschisin gene therapy in photoreceptors, Muller glia or all

- retinal cells in the *Rst1h*<sup>-/-</sup> mouse. *Gene Ther* 2014;21:585–592.
32. Park TK, Wu Z, Kjellstrom S, et al. Intravitreal delivery of AAV8 retinoschisin results in cell type-specific gene expression and retinal rescue in the *Rst1*-KO mouse. *Gene Ther* 2009;16:916–926.
33. Hanitzsch R, Lichtenberger T, Mattig WU. The influence of MgCl<sub>2</sub> and APB on the light-induced potassium changes and the ERG b-wave of the isolated superfused rat retina. *Vision Res* 1996;36:499–507.
34. Robson JG, Frishman LJ. Photoreceptor and bipolar cell contributions to the cat electroretinogram: A kinetic model for the early part of the flash response. *J Opt Soc Am A Opt Image Sci Vis* 1996;13:613–622.
35. Janssen A, Min SH, Molday LL, et al. Effect of late-stage therapy on disease progression in AAV-mediated rescue of photoreceptor cells in the retinoschisin-deficient mouse. *Mol Ther* 2008;16:1010–1017.
36. Ziccardi L, Vijayasathya C, Bush RA, et al. Loss of retinoschisin (RS1) cell surface protein in maturing mouse rod photoreceptors elevates the luminance threshold for light-driven translocation of transducin but not arrestin. *J Neurosci* 2012;32:13010–13021.
37. Xu J, Heys JJ, Barocas VH, et al. Permeability and diffusion in vitreous humor: Implications for drug delivery. *Pharm Res* 2000;17:664–669.
38. Panda-Jonas S, Jonas JB, Jakobczyk M, et al. Retinal photoreceptor count, retinal surface area, and optic disc size in normal human eyes. *Ophthalmology* 1994;101:519–523.
39. Remtulla S, Hallett PE. A schematic eye for the mouse, and comparisons with the rat. *Vis Res* 1985;25:21–31.
40. Jeon CJ, Strettoi E, Masland RH. The major cell populations of the mouse retina. *J Neurosci* 1998;18:8936–8946.
41. Mowat FM, Gornik KR, Dinculescu A, et al. Tyrosine capsid-mutant AAV vectors for gene delivery to the canine retina from a subretinal or intravitreal approach. *Gene Ther* 2014;21:96–105.
42. Dyka FM, Molday RS. Coexpression and interaction of wild-type and missense RS1 mutants associated with X-linked retinoschisis: Its relevance to gene therapy. *Invest Ophthalmol Vis Sci* 2007;48:2491–2497.
43. Vijayasathya C, Sui R, Zeng Y, et al. Molecular mechanisms leading to null-protein product from retinoschisin (RS1) signal-sequence mutants in X-linked retinoschisis (XLRS) disease. *Hum Mutat* 2010;31:1251–1260.

Received for publication October 21, 2015;  
accepted after revision March 31, 2016.

Published online: April 1, 2016.